Effective Density and Volatility of Particles Sampled from a Helicopter Gas Turbine Engine

Jason S. Olfert[1], Matthew Dickau[1], Ali Momenimovahed[2], Meghdad Saffaripour[2], Kevin Thompson[2], Greg Smallwood[2], Marc E. J. Stettler[3,4], Adam Boies[3], Yura Sevcenco[5], Andrew Crayford[5], Mark Johnson[6]

[1] Mechanical Engineering Department, University of Alberta, Edmonton, Canada

[2] Measurement Science and Standards, National Research Council Canada, Ottawa, Canada

[3] Department of Engineering, University of Cambridge, Cambridge, United Kingdom

[4] Centre for Transport Studies, Department of Civil and Environmental Engineering, Imperial College London, London, UK

[5] Cardiff University, Cardiff, Wales CF24 3AA, United Kingdom

[6] Rolls-Royce plc, Derby, United Kingdom

Keywords: gas turbine, particulate emissions, volatility, effective density

Abstract

The effective density and size-resolved volatility of particles emitted from a Rolls-Royce Gnome helicopter turboshaft engine are measured at two engine speed settings (13,000 and 22,000 RPM). The effective density of denuded and undenuded particles were measured. The denuded effective densities are similar to the effective densities of particles from a gas turbine with a double annular combustor as well as a wide variety of internal combustion engines. The denuded effective density measurements were also used to estimate the size and number of primary particles in the soot aggregates. The primary particle size estimates show that the primary particle size was smaller at lower engine speed (in agreement with transmission electron microscopy analysis). As a demonstration, the size-resolved volatility of particles emitted from the engine are measured with a system consisting of a differential mobility analyzer, centrifugal particle mass analyzer, condensation particle counter, and catalytic stripper. This system determines the number distributions of particles that contain or do not contain non-volatile material, and the mass distributions of non-volatile material, volatile material condensed onto the surface of non-volatile particles, and volatile material forming independent particles (*e.g.* nucleated volatile material). It was found that the particulate at 13,000 RPM contained a measurable fraction of purely volatile material with diameters below ~25 nm and had a higher mass fraction of volatile material condensed on the surface of the soot (6–12%) compared to the 22,000 RPM condition (1–5%). This study demonstrates the potential to quantify the distribution of volatile particulate matter and gives additional information to characterize sampling effects with regulatory measurement procedures.

1. Introduction

Particulate emissions from aircraft engines contribute to anthropogenic climate forcing and affect human health (Unal et al. 2005; Woody et al. 2011). Aviation emissions are expected to grow as commercial air traffic is expected to more than double its 2010 levels by the year 2030 (ICAO 2013). Non-volatile particles from aircraft engines typically form as aggregates of carbon primary particles

typically 10–20 nm in diameter (Liati et al. 2014; Boies et al. 2015), bound together in fractal-like branching chain structures. Sizes of such aggregates generally appear in distributions with count median mobility-equivalent diameters of 10 to 40 nm (Kinsey et al. 2010; Boies et al. 2015; Lobo et al. 2015). Here, we will use the term 'soot' to refer to these aggregates excluding any other species (e.g. organics, sulfate, etc.) that may be condensed on it. The relationship between particle mass and particle mobility of the soot is used to convert particle size distributions to particle mass distributions and can provide insight into its morphological properties (e.g. primary particle size; Dastanpour et al. 2016). The mass-mobility relationship is often expressed in term of the particle effective density, defined as the mass divided by the mobility-equivalent volume, which is often measured using a differential mobility analyzer (DMA) with a centrifugal particle mass analyzer (CPMA) or an aerosol particle mass analyzer (APM), and condensation particle counter (CPC). The effective densities of soot are typically found to follow a power-law relationship, with effective density decreasing for increasing mobility-equivalent diameters (Durdina et al. 2014; Johnson et al. 2015; Lobo et al. 2015; Abegglen et al. 2015).

The soot emitted from turbine engines is often mixed with semi-volatile or volatile components generally believed to be sulfate, from sulfur in the fuel, or organic carbon (OC), from exhausted lubricating oil or from the products of incomplete combustion (Timko et al. 2010). The volatile material may exist as pure volatile particles formed via nucleation, or the volatile material may condense onto or envelope non-volatile particles forming particles of the two species. The volatile material existing on the soot or as independent particles can have a significant effect on the particle optical and hygroscopic properties, both of which are important in assessing the climate impact of particulate emissions.

Particle emission regulations are being developed for aircraft given the importance of the emissions in terms of climate and human health. Currently the International Civil Aviation Organization is developing regulations based only on the non-volatile component with a measurement and sampling system described by the Aerospace Information Report 6241 (SAE AIR6241 2013); where the non-volatile particle number is measured with a volatile particle remover and CPC, and the mass of black carbon is measured using laser-induced incandescence or photoacoustic techniques.

The purpose of this work is to determine the effective density and size-resolved volatility of particles emitted from a Rolls-Royce Gnome helicopter turboshaft engine, at two engine speed settings. Firstly, the effective densities of the particles are measured in two states: a denuded state (where all volatile material is removed from the soot) and an undenuded state. The undenuded effective density is needed to determine the volatility of the particles, while the denuded effective density gives the effective density of the soot aggregates. The effective density of the soot provides information on the morphology of the soot aggregates. Previously, only one study has been conducted on the effective density of denuded soot aggregates for turbine engines (Johnson et al., 2015) and no effective density measurements have been conducted on a helicopter turboshaft engine. Secondly, the measurement of the size-resolved volatility of particles is demonstrated using a combination of a DMA, CPMA, CPC, and catalytic stripper. This system quantifies the number and mass distributions of volatile and non-volatile material in the particulate and determines whether the material exists as pure (single-species) particles or multi-species particles.

2. Experimental Setup

The effective density and the size-segregated volatility measurements followed the methodology of Dickau et al. (2016), which is described briefly here. All instruments used in this study are identical to those in Dickau et al. (2016).

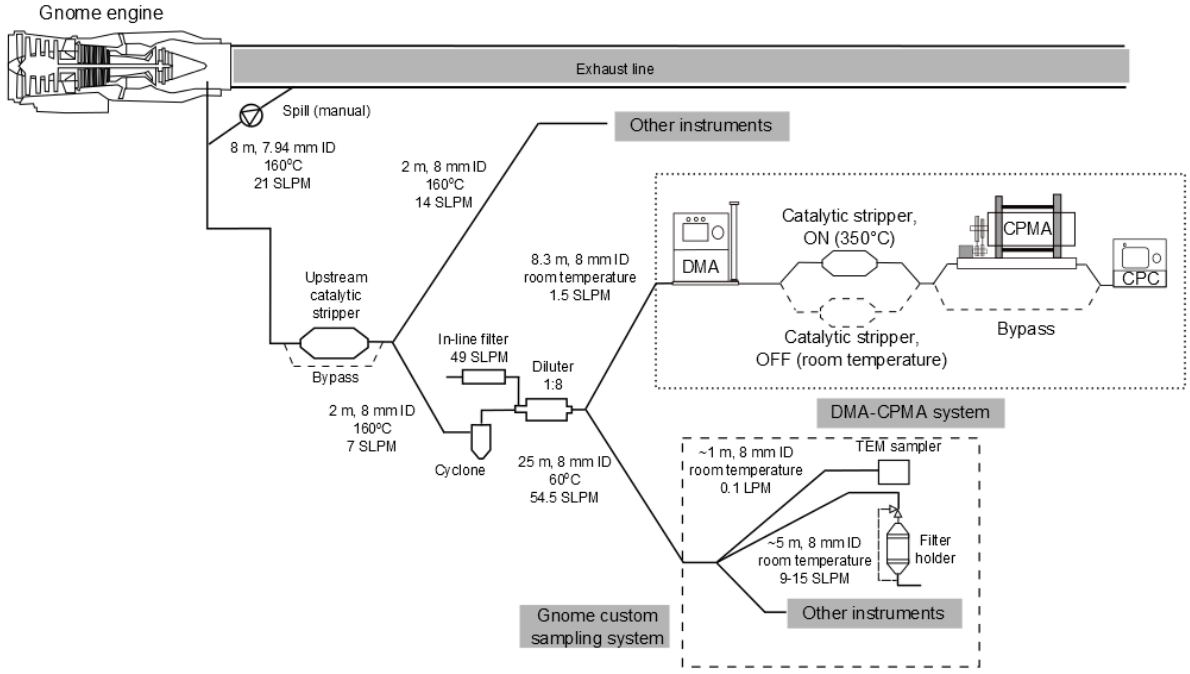

FIGURE 1: Experimental setup for measurements of the volatile mass fraction and volatile particle number fraction, showing the sampling system and the DMA-CPMA setup.

Figure 1 shows the experimental setup used to measure the Gnome particle emissions. These measurements were performed as part of a larger campaign (Mass Assessment of nvPM Technology Readiness for Aviation; MANTRA) and other instruments not relevant to this paper are not shown. The amount of volatile material condensed into the particle-phase will depend on the sampling system. In particular, dilution, sample line temperature, and residence time will all affect homogeneous and heterogeneous nucleation processes in turbine exhaust (Peck et al. 2012). Dilution ratio, sample line temperature, sample flow rate, tube diameters and lengths are shown in Figure 1.

The Gnome engine is a turboshaft helicopter engine of late 1950's design, with a pressure ratio of 8.4 and a maximum power output of 1500 hp. A 2-stage turbine drives a 10 stage axial compressor and has an annular combustor. The free-turbine for driving the load is removed for simpler testbed installation and operation. Engine conditions were varied by controlling the shaft speed from low (13,000 RPM; idle-type) to high (22,000 RPM, near take-off shaft speed) conditions (noting that full take-off power condition was not achievable due to a volume limitation of the exhaust extraction system). The experiments were performed using commercial aircraft Jet A-1 fuel with 17.5% aromatics content and 370 ppm sulfur. The tests were conducted over a period of four days (March 23 – 26, 2015). The

ambient conditions over the test days was relatively consistent ranging between 4 – 9 ^{o}C and a relative humidity of 61% – 81%.

An 8-meter sample line at 160°C was used to transfer the aerosol from the Gnome engine exhaust to a catalytic stripper. A catalytic stripper (Catalytic Instruments, 25 LPM capacity) was placed upstream of the measurement system. For all measurements of volatility presented in this paper, this upstream catalytic stripper was either off or bypassed entirely. Only in the case of measuring the denuded effective density, the upstream catalytic stripper was set to 350°C to remove volatile material prior to measurement. A second heated sample line transferred the aerosol from the upstream catalytic stripper to a diluter (DI-1000; Dekati Ltd, dilution ratio 1:8) using particle-free zero grade nitrogen as the diluent. To remove relatively large particles from the sample, a 1 micron sharp-cut cyclone (Cambustion Ltd) was employed upstream of the diluter. After this, a 2-way splitter provided sample for the DMA-CPMA system, as well as other instruments. The penetration efficiency of the sampling lines from the Gnome engine to the DMA was calculated using the relationship by Gormley and Kennedy (1949) (see the supplementary information, SI). The size distributions shown in this work are an estimate of "engine-out" emissions: the measured size distributions have been corrected for diffusional losses in the sampling lines and for dilution, however, no corrections have been applied for particle coagulation, which would affect the particle size distribution and distribution of volatile material within the aerosol.

In the DMA-CPMA system, the sample aerosol is sent to a differential mobility analyzer (DMA; model 3081, TSI Inc.), which classifies the sample by electrical mobility. The DMA classifies a narrow range of singly-charged particles near the mobility diameter of choice (25 to 250 nm in this study) as well as larger multiply-charged particles with the equivalent electrical mobility. As discussed in the supplementary information, the fraction of multiply-charged particles is relatively small (between 2 – 11% of the particles depending on DMA setting) and the multiply-charged particles have little effect on determining the mass of the singly-charged particles in the CPMA measurements. From the DMA, the sample is then sent through either a catalytic stripper (Model CS015; Catalytic Instruments) heated to 350 °C (with a residence time of ~0.5 s), or through an inactive stripper (Model CS015; Catalytic Instruments) at ambient temperature. The hot stripper removes volatile material from the sample, while the cold stripper leaves the sample unchanged. According to our operational definition of volatility, the volatile material is precisely the material which is removed at 350 °C in the hot catalytic stripper.

To measure the volatile mass fraction, the particles are then sent through the centrifugal particle mass analyzer (Cambustion Ltd), which classifies the sample by mass-to-charge ratio (Olfert and Collings 2005), and finally the number concentration of the particles is measured with a condensation particle counter (CPC; model 3776, TSI Inc.) with an aerosol flow of 1.5 L/min. The CPMA is stepped over a range of mass set points to determine the number of particles present at different masses at the specific mobility selected by the DMA; this data is used to determine the median mass of particles at the DMA mobility-equivalent diameter. The median mass is found by fitting the CPMA data with a log-normal distribution which minimizes the effect of multiply-charged particles (see the SI). The volatile mass fraction is defined as the fraction of volatile material contained in the particle,

$$f_{\mathrm{vm}}(d_{\mathrm{m}}) = 1 - \frac{m_{\mathrm{D}}(d_{\mathrm{m}})}{m_{\mathrm{U}}(d_{\mathrm{m}})}, \quad (1)$$

where d_{m} is the undenuded particle mobility diameter, m_{D} is the median mass of the denuded particles, and m_{U} is the median mass of the undenuded particles. Note that this measurement is independent of the particle losses in the hot or cold stripper, as particle losses in the strippers do not affect the median mass of the distribution measured by CPMA because the particles going through the strippers have the same mobility (Dickau et al., 2016).

To measure the volatile particle number fraction, the sample aerosol is sent through the bypass line instead of the CPMA, and the number concentration is measured by the CPC. The volatile particle fraction (f_{vp}) is the fraction of particles in the aerosol that are only comprised of volatile material (i.e. a pure volatile particle), and is calculated for each particle size selected by the DMA by comparing the number concentrations of the denuded and undenuded particles;

$$f_{\mathrm{vp}}(d_{\mathrm{m}}) = 1 - \frac{n_{\mathrm{D,s}}(d_{\mathrm{m}})}{r_{\mathrm{pen}}(d_{\mathrm{m}})\, n_{\mathrm{U,s}}(d_{\mathrm{m}})} \quad (2)$$

where $n_{\mathrm{D,s}}$ and $n_{\mathrm{U,s}}$ are the measured number concentrations for the denuded and undenuded particle samples, and r_{pen} is the ratio of the penetration efficiency of the hot catalytic stripper to the penetration efficiency of the ambient temperature catalytic stripper. To do this accurately, the differences in penetration losses between the hot and cold strippers had to be characterized; this is done in Dickau et al. (2016). The advantage of using two identical strippers is that the penetration ratio will be close to 1 and thus the uncertainty in the penetration ratio will be small. As shown by Dickau et al. (2016) the penetration ratio ranges between 0.8 to 0.95 and depends on the size of the particle and the penetration ratio has an uncertainty of 3.3% (with 95% confidence).

Measurements of the denuded effective density were made with the upstream catalytic stripper heated to 350°C, in order to remove all volatile material before measurement to determine the effective density of only the non-volatile component of the aerosol, which is expected to be predominately soot.

The number distribution was also measured using a scanning mobility particle sizer: differential mobility analyzer (DMA; model 3081, TSI Inc.) with sheath flow of 15 L/min and a condensation particle counter (CPC; model 3776, TSI Inc.) with an aerosol flow of 1.5 L/min. The size distribution is calculated from this data using the inversion routine in the TSI AIM software (version 9), without diffusion and multiple-charge correction.

Transmission electron microscopy (TEM) and thermal-optical analysis (TOA) was also performed and these experimental procedures are described in the SI.

3. Results

3.1 Effective density: Relationship between particle mass and mobility

The relationship between the particle mass and particle mobility must be known in order to calculate the mass distribution of an aerosol. The relationship between mass and moblity is often express with the effective density, which is defined as the mass of the particle divided by its mobility equivalent volume. For non-spherical particles, the effective density is a function of mobility diameter and is typically expressed as a power-law fit of experimental data (Park et al. 2003):

$$\rho_{\mathrm{eff}}(d_{\mathrm{m}}) = \frac{m}{\frac{\pi}{6} {d_{\mathrm{m}}}^3} = C\, {d_{\mathrm{m}}}^{D_{\mathrm{m}}-3}, \tag{3}$$

where *C* is a constant pre-factor and D_{m} is the mass-mobility exponent. The effective density is determined by selecting particles with the DMA and measuring their mass with the CPMA. The effective density of the undenuded particulate for the Gnome engine is shown in Figure 2. In these experiments the catalytic strippers upstream and downstream of the DMA were not used and the measurements represent the effective density of the particles including any volatile material condensed on the surface. The power-law relationships based on the fit of the data are shown in the figure and these relationships are used to calculate the mass distributions shown in Section 3.2.2. The error bars in the figure (and all subsequent figures) represent 95% confidence intervals of the uncertainty in the measurement. The uncertainty analysis for all measurements is shown in the supplementary information.

Figure 2 also shows a comparison of the effective densities measured for undenuded soot from the Gnome engine to that of undenuded soot from a CFM56-5B4/2P (Lobo et al. 2015) and a CFM56-7B26/3 (Abegglen et al. 2015; Durdina et al. 2014). The dark shaded region is the range bounded by Abegglen et al. (2015) fit curves from 22% engine thrust (lower boundary) to 118% thrust (upper boundary). The light shaded region is the range bounded by Durdina et al. (2014) fit curves from 3% thrust (lower boundary) to 100% thrust (upper boundary). Undenuded effective densities measurements are sensitive to the sampling system used to condition the particles due to the effect volatile material has on the mass of the particles. Although volatile material tends to have material densities lower than soot, the presence of small amounts of volatile material on soot tends to increase the effective density of the particles by filling voids in the soot — increasing the particle's mass without measurably changing the particle's mobility diameter (Ghazi et al. 2013). In the case of large amounts of volatile material, the mass of volatile material greatly outweighs the mass of soot, the particle becomes spherical, and the effective density approaches the material density of the volatile material.

Lobo et al. (2015) used a similar dilution system (with dilution ratio of ~10) and their effective density data is similar to the measurements from the Gnome engine. On the other hand, Abegglen et al. (2015) and Durdina et al. (2015) did not dilute their sample for the majority of their tests but used a dryer to remove water from the aerosol. (In comparison tests, Durdina et al. (2015) found that at high thrust the effective densities of diluted and undiluted samples were similar). Abegglen et al. (2015) and Durdina et al. (2015) data overlap each other significantly, and for the most part they lie above the measurements from the Gnome engine and Lobo et al. (2015). The differences in the effective densities could be due to differences in the soot structure (i.e. primary particle size) due to differences in engine technologies or due to the amount of volatile material condensed on the surface of the soot which will also be a function of the particle sampling system used in each experiment.

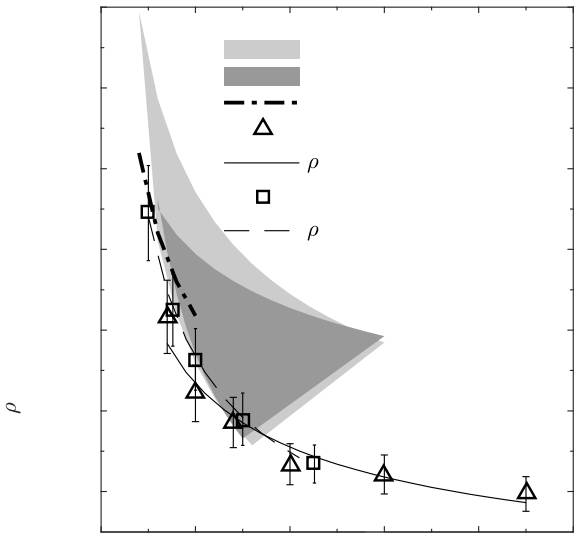

FIGURE 2: Comparison of the effective densities of undenuded Gnome engine particulate to that of a CFM56-5B4/2P turbine (Lobo et al. 2015) and a CFM56-7B26/3 (Abegglen et al. 2015, Durdina et al. 2014). The constant *C* in the effective density functions has units of $\mathrm{kg\ nm}^{-D_m}$.

Effective density measurements were also conducted where the particulate was denuded upstream of the DMA. In this case, the effective density of the aggregate soot particles is determined which provides insight into thier morphology, and as the volatile material is removed from the soot, the measurement should be insensitive to the sampling system conditions allowing for a comparision between engine technologies. Figure 3 shows the effective density measurements for the Gnome engine soot at the 13,000 RPM and 22,000 RPM settings with power-law fits to the data. The supplementary information contains tests that demonstrate the effectiveness of the upstream catalytic stripper to remove volatile material from the soot. The results show that essentially all (>95% by mass fraction) of the volatile material was removed from the soot.

Systematic differences between the effective densities of denuded and undenuded soot are difficult to judge given the large uncertainties in the measurements (due to day-to-day variability in the experiment). For the 22,000 RPM setting, the denuded measurements are ~9% higher on average. For the 13,000 RPM setting, the effective density of particles denuded upstream of the DMA is on average 15% lower than the density of the undenuded particles. Although the uncertainty is large, the reduction in the effective density of the particles may be due to the removal of volatile material which may have filled the voids in the soot (increasing particle mass with little change in the particle mobility). This is explored more fully in Section 3.2 which shows the mass fraction of volatile material condensed on the soot as a function of mobility size.

Figure 3 also shows a comparison of the effective densities measured for denuded soot from the Gnome engine to that of denuded soot from a CFM56-5B4/2P turbine (Johnson et al. 2015) which is the only data in the literature with denuded effective density measurements of soot from a turbine. The CFM56-5B4/2P turbine has a double annular combustor. The data from the CFM56-5B4/2P turbine are at thrusts between 10 – 31% of maximum where the turbine is operating only with the pilot stage combustor and low local air-to-fuel ratios (Boies et al. 2015), and hence may not be typical of modern turbines. The densities measured for the Gnome engine decrease with increasing mobility diameter faster than Johnson's data; however, the measurements are within ~20% of each other, even though the engine technology is substantially different. Johnson et al. (2015) found that the effective density of the soot increased slightly with increased thrust and the same trend is found on the Gnome turbine since the 22,000 RPM effective densities are greater than the 13,000 RPM measurements.

Figure 3 also shows a shaded region representing effective densities measured from several internal combustion engines as compiled by Graves (2015). The Graves (2015) data is a plot of Eq (3) with C=0.131 kg m$^{-2.49}$ and D_m = 2.49 with a shaded region (representing $\pm$27% of the fit) that contains 90% of the effective density measurements of denuded soot, or soot known to contain little volatile material, from several sources including: Diesel engines (Park et al. 2003; Maricq and Xu 2004; Olfert et al. 2007), gasoline direct injection engines (Momenimovahed and Olfert 2015; Quiros et al. 2015; Graves et al. 2017), a port injected gasoline engine (Quiros et al. 2015), and a natural gas direct-injection compression-ignition engine (Graves et al. 2015). Several of these studies show that the effective density of denuded soot does systematically vary with engine conditions (*e.g.* power) and these changes tend to be typically less than 30%, while the effective density of undenuded engine soot can have much higher degrees of variability (*e.g.* Johnson et al. 2015; Momenimovahed and Olfert 2015; Graves et al. 2015). There is little doubt that there are systematic differences in the morphologies of gas turbine and internal combustion engine soot; although, it is interesting that the Gnome and CFM56-5B4/2P engine soot denuded effective densities are broadly similar to soot from internal combustion engines. Future work is required to measure the denuded effective density of modern gas turbines.

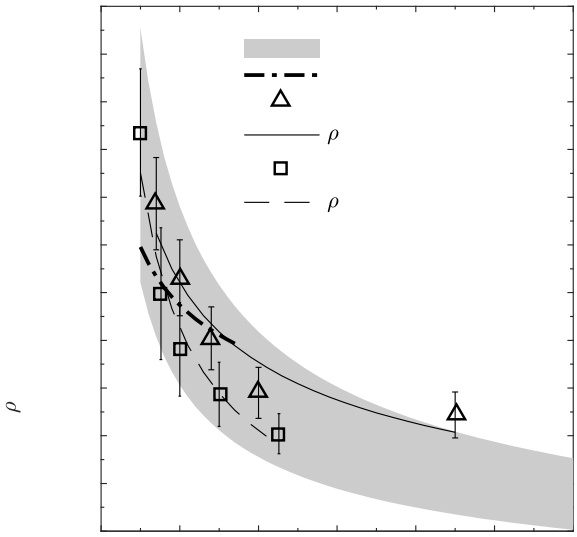

FIGURE 3: Comparison of the effective densities of denuded Gnome engine particulate to that of a CFM56-5B4/2P turbine (Johnson et al. 2015) and a summary of effective densities from a wide range of internal combustion engines (Graves, 2015). The constant *C* in the effective density functions has units of $\mathrm{kg\,nm^{-D_m}}$.

Systematic differences in the effective density of aggregate soot particles can be explained by differences in the size and number of the primary particles within the aggregate (Eggersdorfer et al. 2012) and the scaling of primary particle size with aggregate size (smaller aggregates tend to have smaller primary particle sizes, Dastanpour and Rogak 2014). Primary particle size is an important parameter in understanding soot's impact on climate and health as it has a strong influence on the light scattering, absorption, and surface area of a soot aggregate. As shown in Figure 3, the effective density of soot at 22,000 RPM is consistently higher than the soot at 13,000 RPM for a given mobility size, implying that the 22,000 RPM soot has a larger primary particle size. An increase in the primary particle size with increasing engine thrusts has also been observed by Liati et al. (2014) and Durdina et al. (2014).

The surface-area mean (Sauter) primary particle diameter was calculated using the denuded effective density functions given in Figure 3 using the scaling relationship given by Eggersdorfer et al. (2012) and using scaling exponents given by Dastanpour et al. (2016) for soot (D_α=1.1; k_α=1.13). Figure 4 shows the primary particle diameters calculated using these relationships which have an uncertainty of at least 20% (Dastanpour et al. 2016). The figure shows that the primary particle size of the soot from the 22,000 RPM condition has a larger primary particle diameter and this difference increases with an increase in aggregate mobility diameter. An analysis of primary particle diameter was also conducted using transmission electron microscopy (TEM). The *mean* projected-area equivalent primary particle diameter was found to be 17.2 nm (with a standard deviation of σ=3.5 nm and sample size of *n*=61 randomly selected primary particles in several randomly selected aggregates) at 13,000 RPM; and 21.5 nm (σ=5.3 nm, *n*=50) at 22,000 RPM. Although these numbers are difficult to compare to the DMA-

CPMA analysis, the TEM analysis also suggests that the mean primary particle size is larger at 22,000 RPM.

The inset of Figure 3 shows the number of primary particles contained in each aggregate as a function aggregate mobility diameter calculated using the relationships of Eggersdorfer et al. (2012) and Dastanpour et al. (2016) described above. Since the diameter of the primary particles decreases with the size of the aggregate, even small aggregates may contain several primary particles. The figure shows that even for the smallest aggregates studied by DMA-CPMA analysis (25 nm at 13, 000 RPM; and 35 nm at 22, 000 RPM), there are approximately 10 primary particles, which suggests there is void space into which volatile material can condense. This explains why the effective density of undenuded soot at 13,000 RPM can be higher than the denuded soot even for small aggregates.

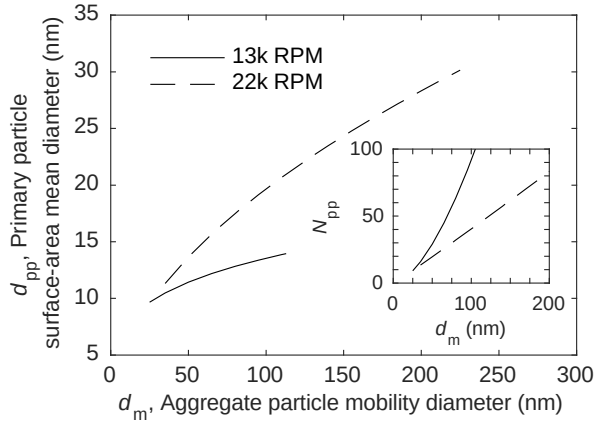

FIGURE 4: Surface-area mean diameter of the primary particles forming the aggregates as a function of the mobility diameter of the aggregate particles. The inset shows the average number of primary particles (N_{pp}) in each aggregate as a function of aggregate mobility diameter.

3.2 Volatility Measurements

In the following sections volatility measurements from the Gnome helicopter engine are presented as a demonstration. As noted above, the amount of semi-volatile material measured in the particle-phase will not only be a function of the engine operating conditions, but also the sampling system. Factors such as dilution ratio, sample line temperature, and residence time are all expected to affect the partitioning of semi-volatile material into the gas or aerosol phase. As the sampling conditions used here are quite different from natural atmospheric processes, it is not expected that the volatility measurements would be reflective of particle emissions in the atmosphere. Nevertheless, the sampling system used here is similar in some ways to the AIR6241 system which is characterized by low dilution ratios and long heated sampling lines. The measurements shown below describe how the semi-volatile aerosol material is distributed within the aerosol, i.e., either as independent, purely volatile particles or as volatile material condensed on the surface of non-volatile particle. This provides some insight into their formation.

3.2.1 Volatile Particle Number Fraction and Number Distributions

Figure 5 shows the volatile number fractions of the Gnome engine particle emissions, at 13,000 RPM and 22,000 RPM (i.e. the number fraction of purely volatile particles as a function of mobility diameter). For the soot at 13,000 RPM, the volatile number fraction was over 40% for 13 nm particles, decreasing down to around 5% for large particles. The soot at 22,000 RPM has volatile number fractions around 5-10%, showing a slight decrease with increasing particle size. Approximately 5% of the particles greater than 50 nm at both engine settings were measured to be volatile although this is close to the uncertainty level of the method as seen by the error bars.

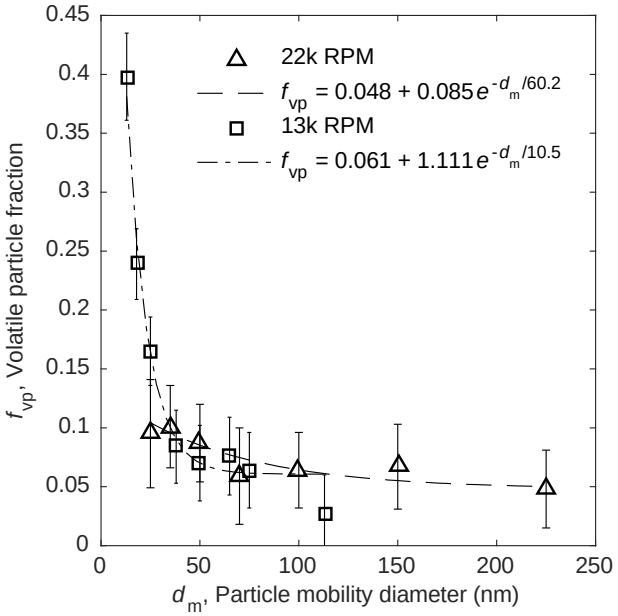

FIGURE 5: Volatile particle number fraction as a function of particle mobility diameter for particulate from a Gnome engine at 22,000 RPM and 13,000 RPM.

As a demonstration, the volatile particle fraction is used to calculate the number distributions of the particulate segregated in terms of particle that are only composed of volatile material (labelled 'pure volatile' in the figure legend) or particles that contain at least some non-volatile material ('Non-volatile'). These distributions are calculated from the total size distribution measured by the SMPS (using one SMPS measurement as an demonstration), $\frac{\mathrm{d}N}{\mathrm{d}\log d_\mathrm{m}}(d_\mathrm{m})$, and the volatile particle fractions, $f_\mathrm{vp}(d_\mathrm{m})$, shown in Figure 6. Specifically, the number distribution of particles that contain a non-volatile component, $\mathrm{d}N_\mathrm{nv}/\mathrm{d}\log d_\mathrm{m}$, is;

$$\frac{\mathrm{d}N_\mathrm{nv}}{\mathrm{d}\log d_\mathrm{m}}(d_\mathrm{m}) = \Big(1 - f_\mathrm{vp}(d_\mathrm{m})\Big)\frac{\mathrm{d}N}{\mathrm{d}\log d_\mathrm{m}}(d_\mathrm{m}) \tag{4}$$

and the number distribution of particles that are solely volatile, $\mathrm{d}N_\mathrm{v}/\mathrm{d}\ln d_\mathrm{m}$, is;

$$\frac{\mathrm{d}N_\mathrm{v}}{\mathrm{d}\log d_\mathrm{m}}(d_\mathrm{m}) = f_\mathrm{vp}(d_\mathrm{m})\frac{\mathrm{d}N}{\mathrm{d}\log d_\mathrm{m}}(d_\mathrm{m}). \tag{5}$$

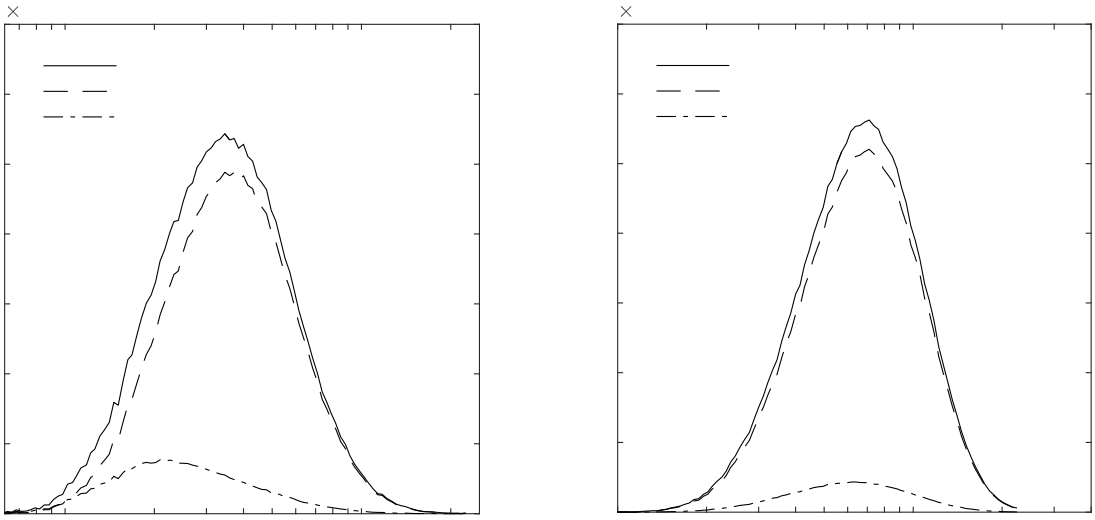

FIGURE 6: Number distributions of Gnome engine particulate from a) the 13,000 RPM condition and b) the 22,000 RPM condition, showing the number distribution of particles only consisting of volatile material (Eq. 5; 'Pure volatile' in the legend), the number distribution of particles containing volatile material (Eq. 4; 'Non-volatile'), and the number distribution of the total aerosol ('Total concentration').

Figure 6 shows that vast majority of the particles emitted by the engine contain non-volatile material. The figures reveal a small amount of pure volatile particles above 50 nm for each engine setting; however, as shown in Figure 5 this is close to the uncertainty in the measurement and may simply be experimental error. At the 13,000 RPM setting, there is a small, but measurable, amount of purely volatile particles below 25 nm. Purely volatile nucleation mode particles have been observed in aircraft exhaust, but they generally have a size less than 20 nm (Wey et al. 2006).

3.2.2 Volatile Mass Fraction and Mass Distributions

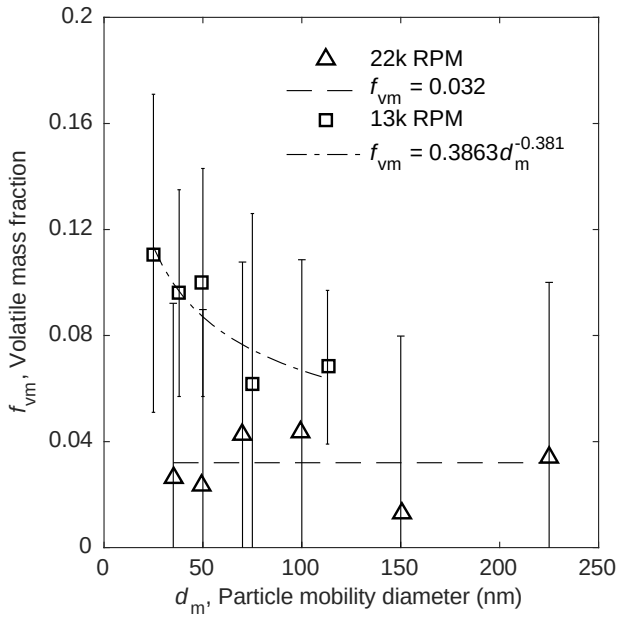

FIGURE 7: Volatile mass fraction as a function of particle mobility diameter for particulate from a Gnome engine at 22,000 RPM and 13,000 RPM.

Figure 7 shows the volatile mass fractions of the Gnome engine particles, at 13,000 RPM and 22,000 RPM. At 13,000 RPM, the particles have volatile mass fractions in the range of 6-12%, gradually decreasing with increasing size. An uncertainty analysis is shown in the supplementary information which shows that the large confidence intervals is due to a low sample size and measurement uncertainty and also day-to-day variability of the experiment which was measured in three tests over three days.

A decreasing trend in volatile mass fraction as a function of mobility-equivalent diameter has also been observed for particles from diesel engines (Sakurai et al. 2003; Ristimäki et al. 2007), gasoline direct injection engines (Momenimovahed and Olfert 2015), a natural gas direct-injection compression-ignition engine (Graves et al., 2015), as well as pre-mixed flames (*e.g.* McKenna burner; Ghazi et al. 2013) and diffusion flames (e.g. mini-CAST; Dickau et al. 2016). As shown by Ristimäki et al. (2007) a decreasing trend in volatile mass fraction at 13,000 RPM is expected if the volatile material condensed on the soot through condensational growth. Condensational growth requires supersaturation of the volatile species which would be expected as the exhaust cools in the sample line if the concentration of volatile species in the exhaust was sufficiently high.

The soot at 22,000 RPM has volatile mass fractions ranging around 1-5% without any apparent trend with respect to particle size. A small size-independent volatile mass fraction is expected if the main phenomena resulting in mass transfer to the soot was due to physical adsorption as shown by Ristimäki et al. (2007). In this case, supersaturation is not necessary and adsorption may take place within the hot

exhaust. Another factor may be particle coagulation in the sampling lines. Purely volatile particles in the sampling lines may coagulate with non-volatile particles to form mixed particles.

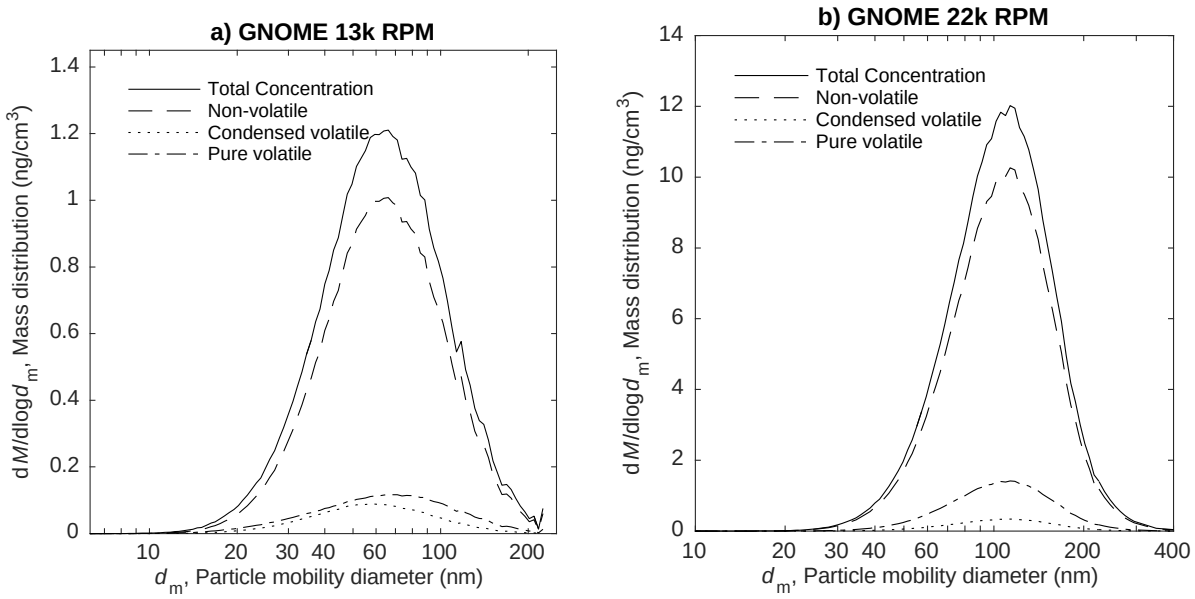

FIGURE 8: Mass distributions of Gnome engine particulate from a) the 13,000 RPM condition and b) the 22,000 RPM condition, showing the mass distribution of the components as a function of the mobility of the undenuded particles, including the mass distribution of particles only consisting of volatile material (Eq. 8; 'Pure volatile' in the legend), the mass distribution volatile material condensed on the surface of non-volatile material (Eq. 7; 'Condensed volatile'), the mass distribution of volatile material condensed on the surface of non-volatile material (Eq. 7; 'Condensed volatile'), the mass distribution of non-volatile material (Eq. 6; 'Non-volatile'), and the mass distribution of the total aerosol ('Total concentration').

In Figure 8, the mass distributions are calculated from the total size distribution measured by the SMPS, $\frac{\mathrm{d}N}{\mathrm{d}\log d_\mathrm{m}}(d_\mathrm{m})$, the volatile mass fractions $f_\mathrm{vm}(d_\mathrm{m})$ shown in Figure 7, and the mass of the particles from the effective density measurement shown in Figure 2. The mass distribution of the non-volatile component of the aerosol as a function of the undenuded mobility diameter is;

$$\frac{\mathrm{d}M_\mathrm{nv}}{\mathrm{d}\log d_\mathrm{m}}(d_\mathrm{m}) = \left(1 - f_\mathrm{vm}(d_\mathrm{m})\right)\frac{\pi}{6} d_\mathrm{m}^3 \rho_\mathrm{eff}(d_\mathrm{m}) \left(1 - f_\mathrm{vp}(d_\mathrm{m})\right) \frac{\mathrm{d}N}{\mathrm{d}\log d_\mathrm{m}}(d_\mathrm{m}) \quad (6)$$

where the term $\frac{\pi}{6} d_\mathrm{m}^3 \rho_\mathrm{eff}(d_\mathrm{m})$ is the median mass of the particles that contain both volatile and non-volatile material and is determined from the functions shown in Figure 2. The mass distribution of the volatile component condensed on non-volatile particles is,

$$\frac{\mathrm{d}M_\mathrm{cond}}{\mathrm{d}\log d_\mathrm{m}}(d_\mathrm{m}) = f_\mathrm{vm}(d_\mathrm{m})\frac{\pi}{6} d_\mathrm{m}^3 \rho_\mathrm{eff}(d_\mathrm{m}) \left(1 - f_\mathrm{vp}(d_\mathrm{m})\right) \frac{\mathrm{d}N}{\mathrm{d}\log d_\mathrm{m}}(d_\mathrm{m}) \quad (7)$$

And the mass distribution of the purely volatile particles is,

$$\frac{\mathrm{d}M_{\mathrm{pure}}}{\mathrm{d}\log d_{\mathrm{m}}}(d_{\mathrm{m}}) = \frac{\pi}{6} d_{\mathrm{m}}^3 \rho_{\mathrm{vol}} f_{\mathrm{vp}}(d_{\mathrm{m}}) \frac{\mathrm{d}N}{\mathrm{d}\log d_{\mathrm{m}}}(d_{\mathrm{m}}) \quad (8)$$

where the term $\frac{\pi}{6} d_{\mathrm{m}}^3 \rho_{\mathrm{vol}}$ is the mass of the pure volatile particles. Theoretically, the mass of the pure volatile particles would be measured in the DMA-CPMA system. However, if the concentration of the pure volatile particle is small with respect to the concentration of the particles containing both species (which is the case here) or if the effective densities of the purely volatile particles and multi-component particles is similar, then the mass of the pure volatile particles cannot be resolved with the DMA-CPMA system (see Dickau et al. 2016 for details). Therefore, we have assumed that the density of the pure volatile particles is 1000 kg/m^3, which is near the density of mixtures of aliphatic and polycyclic aromatic hydrocarbons and other volatile material (Slowik et al. 2007). As the mass fraction of pure volatile particles is small (see Table 1), this assumption introduces little error into the total mass concentration.

Table 1: Total mass fractions for the different components of the particulate at different engine conditions

	22,000 RPM	**13,000 RPM**
Non-volatile component	85%	82%
Volatile component condensed on non-volatile particles	3%	7%
Pure volatile particles	12%	11%

These curves can be integrated to give the total mass fractions for each component of the particulate, as shown in Table 1. Both mass distributions show that the majority of the mass of the particulate is in the non-volatile component. Furthermore, the particulate from the 22,000 RPM setting shows only a very small proportion (3% by mass) of volatile material attached to non-volatile particles. There is a measureable mass of pure volatile particles at both engine conditions. For the 13,000 RPM setting, there is a measureable amount volatile material attached to non-volatile particles (7% by mass), and again some purely volatile particles. The primary difference between the two conditions is the increased amount of volatile material attached to non-volatile particles in the 13,000 RPM setting. It is important to note that although the 13,000 RPM condition contains a significantly higher volatile mass fraction and volatile particle number fraction, this makes very little difference in the total volatile to non-volatile mass ratio. This is because the additional volatile material occurs at smaller particle sizes which contribute very little to the total mass concentration.

Nine filters for thermal-optical analysis were also taken at 22,000 RPM to compare to the relative mass concentrations measured by the DMA-CPMA system. The thermal-optical analysis found that the relative proportion of organic carbon to total carbon (organic carbon and elemental carbon) was 0.20±0.11. Assuming that all non-volatile material is elemental carbon and that all volatile material is organic carbon, the DMA-CPMA system measures 0.15 (Table 1) which agrees reasonably well to the thermal-optical analysis given the relatively large uncertainties in both methods when the proportion of volatile material or organic carbon is small.

4. Conclusion

Effective density measurements of denuded soot provide insight into the morphology of the soot aggregates. Although the denuded effective densities of the Gnome particulate did depend on shaft speed, they were similar (within approximately ±20%) to those found by Johnson et al. (2015) for a gas turbine with a double annular combustor. The denuded effective densities are also similar (within approximately ±30%) with effective densities from a wide range of internal combustion engines. Future work is needed to measure the denuded effective density of modern gas turbines. Perhaps a single effective density relationship could be used to estimate denuded effective densities if direct measurement were not possible.

It was also demonstrated how the DMA-CPMA system can be used to determine the volatility of particle emissions sampled from a gas turbine. It was shown that the system can measure non-volatile particle number and mass concentrations, which AIR6241-compliant instruments also measure, but with the added benefit of also measuring volatile number and mass concentrations as well as providing mass and number concentrations on a size-segregated basis. The DMA-CPMA system would not be appropriate for regulatory measurement as it is not a real-time measurement system; however, the measurements maybe useful for research applications such as characterizing the distribution of volatile material in the particulate (*e.g.* nucleation-mode particles vs. particles coated with volatile material), measuring the volatile coating on soot particles (*e.g.* to investigate if coating affects measurements by AIR6241-compliant mass instruments), characterizing dilution or sample-line temperature effects on particle volatility, or others.

Acknowledgements

Funding for this research was provided by Transport Canada, National Sciences and Engineering Research Council, Alberta Innovates Technology Futures, and Cambustion Ltd. We wish to acknowledge Catalytic Instruments for providing the catalytic strippers, European Aviation Safety Agency for providing the particle sampling system, and especially Rolls-Royce for hosting the campaign where these measurements were taken.

References

Abegglen, M., Durdina, L., Brem, B.T., Wang, J., Rindlisbacher, T., Corbin, J.C., Lohmann, U., Sierau, B. (2015). Effective density and mass–mobility exponents of particulate matter in aircraft turbine exhaust: Dependence on engine thrust and particle size. Journal of Aerosol Science, 88, 135-147.

Boies, A., Stettler, M., Swanson, J., Johnson, T., Olfert, J., Johnson, M., ... Rogak, S. (2015). Particle Emissions Characteristics of a Gas Turbine with a Double Annular Combustor. Aerosol Science and Technology, 49(9), 842-855.

Dastanpour, R., Rogak, S. N., Graves, B., Olfert, J., Eggersdorfer, M. L., Boies, A. M. (2016). Improved sizing of soot primary particles using mass-mobility measurements. Aerosol Science and Technology, 50(2), 101-109.

Dastanpour, R., and Rogak, S. N. (2014). Observations of a Correlation between Primary Particle and Aggregate Size for Soot Particles. Aerosol Science and Technology. 48(10): 1043–1049.

Dickau, M., Olfert, J., Stettler, M., Boies, A., Momenimovahed, A., Thomson, K., Smallwood, G., Johnson, M. (2016). Methodology for Quantifying the Volatile Mixing State of an Aerosol, Aerosol Science and Technology, 50(8), 759-772.

Durdina, L., Brem, B.T., Abegglen, M., Lobo, P., Rindlisbacher, T., & Thomson, K.A., et al. (2014). Determination of PM mass emissions from an aircraft turbine engine using particle effective density. Atmospheric Environment, 99, 500–507,

Eggersdorfer, M. L., Kadau, D., Herrmann, H. J., Pratsinis, S. E. (2012). Aggregate morphology evolution by sintering: Number and diameter of primary particles. *Journal of Aerosol Science*, 46, 7-19.

Ghazi, R., Tjong, H., Soewono, A., Rogak, S. N., and Olfert, J. S. (2013). Mass, mobility, volatility, and morphology of soot particles generated by a McKenna and inverted burner. Aerosol Science and Technology, 47(4), 395-405.

Gormley, P. G., Kennedy, M. (1949). Diffusion from a stream flowing through a cylindrical tube. *Proceedings of the Royal Irish Academy*, 52A, 163–169.

Graves. B. (2015). *Characterization of Particulate Matter Morphology and Volatility for Two Direct-Injection Engines*. Master of Science thesis. University of Alberta.

Graves. B., Koch, C. R., Olfert, J. S. (2017). Morphology and Volatility of Particulate Matter Emitted from a Gasoline Direct Injection Engine Fueled on Gasoline and Ethanol Blends. *Journal of Aerosol Science,* 105, 166-178.

Graves, B., Olfert, J. S., Patychuk, B., Dastanpour, R. & Rogak, S. (2015). Characterization of Particulate Matter Morphology and Volatility from a Compression-Ignition Natural-Gas Direct-Injection Engine. *Aerosol Science & Technology* 49(8), 589-598.

International Civil Aviation Organization. (2013) ICAO 2013 Environmental Report. Accessed online at http://cfapp.icao.int/Environmental-Report-2013/files/assets/common/downloads/ICAO_2013_Environmental_Report.pdf

Johnson, T., Olfert, J., Symonds, J., Johnson, M., Rindlisbacher, T., Swanson, J., et al. (2015). Effective density and mass-mobility exponent of aircraft turbine particulate matter. Journal of Propulsion and Power, 31(2), 573-581.

Kinsey, J.S., Dong, Y., Williams, D.C., and Logan,R. Physical characterization of the fine particle emissions from commercial aircraft engines during the Aircraft Particle Emissions eXperiment (APEX) 1–3, Atmos Env, 44(17), 2147-2156,

Liati, A., Brem, B.T., Durdina, L., Vögtli, M., Dasilva, Y. A. R., Eggenschwiler, P. A. & Wang, J. (2014). Electron Microscopic Study of Soot Particulate Matter Emissions from Aircraft Turbine Engines. Environmental Science & Technology, 48 (18), 10975–10983.

Lobo, P., Durdina, L., Smallwood, G., Rindlisbacher, T., Siegerist, F., Black, E., et al. (2015). Measurement of Aircraft Engine Non-Volatile PM Emissions: Results of the Aviation-Particle Regulatory Instrumentation Demonstration Experiment (A-PRIDE) 4 Campaign. Aerosol Science and Technology, 49(7), 472-484.

Maricq, M., and Xu, N. (2004). The Effective Density and Fractal Dimension of Soot Particles from Premixed Flames and Motor Vehicle Exhaust. Journal of Aerosol Science. 35: 1251–1274.

Momenimovahed, A. & Olfert, J. S. (2015). Effective Density and Volatility of Particles Emitted from Gasoline Direct Injection Vehicles and Implications for Particle Mass Measurement. Aerosol Science & Technology 49(11), 1051-1062.

NIOSH. (2003). Monitoring of Diesel Particulate Exhaust in the Workplace, Chapter Q, Third Supplement to NMAM, in NIOSH Manual of Analytical Methods, 4th ed., P. F. O'Connor, P. C. Schlecht, eds., NIOSH, Cincinnati, OH, USA. NIOSH DHHS Publication No. 2003-154

Olfert, J. S., & Collings, N. (2005). New method for particle mass classification—the Couette centrifugal particle mass analyzer. Journal of Aerosol Science, 36(11), 1338–1352.

Olfert, J. S., Symonds, J., and Collings, N. (2007). The Effective Density and Fractal Dimension of Particles Emitted from a Light-Duty Diesel Vehicle with a Diesel Oxidation Catalyst. Journal of Aerosol Science. 38: 69–82.

Park, K.,Cao, F.,Kittelson, D. B., McMurry, P. H. (2003). Relationship between Particle Mass and Mobility for Diesel Exhaust Particles. *Env Sci & Tech,* 37(3), 577-583.

Peck, J., Timko, M.T., Yu, Z., Wong, H.-W., Herndon, S.C., Yelvington, P.E., Miake-Lye, R.C., Wey, C., Winstead, E.L., Ziemba. L.D., and Anderson, B.E. (2012). Measurement of Volatile Particulate

Matter Emissions from Aircraft Engines Using a Simulated Plume Aging System. ASME. *J. Eng. Gas Turbines Power.* 134(6):061503-061503-8.

Petzold, A., Ogren, J. A., Fiebig, M., Laj, P, Li, S.-M., Baltensperger, U., Holzer-Popp, T., Kinne, S., Pappalardo, G., Sugimoto, N., Wehrli, C., Wiedensohler, A. and Zhang, X.-Y.. (2013). Recommendations for reporting "black carbon" measurements. Atmospheric Chemistry and Physics, 13, 8365-8379.

Quiros, D., Hu, S. [Shaohua], Hu, S. [Shishan], Lee, E., Sardar, S., Wang, X., Olfert, J. Jung, H., Zhu, Y., and Huai, T. (2015). Particle Effective Density and Mass During Steady-State Operation of GDI, PFI, and Diesel Passenger Cars. Journal of Aerosol Science. 83: 39–54.

Ristimäki, J., Vaaraslahti, K., Lappi, M., and Keskinen, J. (2007). Hydrocarbon Condensation in Heavy-Duty Diesel Exhaust. Environ. Sci. Technol., 41:6397–6402.

SAE Aerospace Information Report 6241. (2013). *Procedure for the Continuous Sampling and Measurement of Non-Volatile Particle Emissions from Aircraft Turbine Engines*. SAE International, Warrendale, PA.

Sakurai, H., Park, K., McMurry, P. H., Zarling, D. D., Kittleson, D. B., and Ziemann, P. J. (2003). Size-Dependent Mixing Characteristics of Volatile and Nonvolatile Components in Diesel Exhaust Aerosols. Environ. Sci. Technol., 37:5487–5495.

Slowik, J. G., Cross, E. S., Han, J.-H., Davidovits, P., Onasch, T. B., Jayne, J. T., et al. (2007). An Inter-Comparison of Instruments Measuring Black Carbon Content of Soot Particles. Aerosol Sci. Technol., 41:295–314.

Timko, M.T., Onasch T.B., Northway MJ, Jayne, J.T., Canagaratna, M.R., Herndon, S.C., Wood, E.C., Miake-Lye, R.C., and Knighton, W.B. Gas Turbine Engine Emissions—Part II: Chemical Properties of Particulate Matter. ASME. *J. Eng. Gas Turbines Power.* 2010;132(6):061505-061505-15.

Unal, A., Hu, Y. T., Chang, M. E., Odman, M. T., and Russell, A. G., Airport Related Emissions and Impacts on Air Quality: Application to the Atlanta International Airport, *Atmospheric Environment*, Vol. 39, No. 32, 2005, pp. 5787–5798.

Wey, C. C., Anderson, B. E., Wey, C., Li-Jones, X., Winstead, E., Thornhill, L. K. et al., “Aircraft Particle Emissions Experiment (APEX),” NASA TM-2006-214382, 2006.

Woody, M., Baek, B. H., Adelman, Z., Omary, M., Lam,Y. F.,West, J. J., and Arunachalam, S., “An Assessment of Aviation’s Contribution to Current and Future Fine Particulate Matter in the United States,” *Atmospheric Environment*, Vol. 45, No. 20, 2011, pp. 3424–3433.